Relaxation effects in inner-shell photoionization of Mg, Ca, and Sr

M. Kutzner, V. Maycock,* J. Thorarinson, E. Pannwitz, and J. A. Robertson†
Department of Physics, Andrews University, Berrien Springs, Michigan 49104
(Received 28 June 2001; revised manuscript received 25 July 2002; published 23 October 2002)

Total and partial photoionization cross sections have been calculated for all inner subshells of atomic magnesium, calcium, and strontium in the relativistic random-phase approximation, the relativistic random-phase approximation modified to include relaxation effects, and the relativistic random-phase approximation modified to include relaxation and Auger decay. Results of the three models are compared with Dirac-Hartree-Fock calculations and with semiempirical results so that the import of various many-body effects can be assessed. Branching ratios and photoelectron angular-distribution asymmetry parameters are also presented for *np* subshells. Substantial relaxation effects are noted for photoionization of $1s$ and $2s$ subshells.

DOI: 10.1103/PhysRevA.66.042715 PACS number(s): 32.80.Fb

I. INTRODUCTION

Valence photoionization of the alkaline-earth-metal atoms magnesium ($Z=12$), calcium ($Z=20$), and strontium ($Z=38$) has attracted much attention in recent decades. The double-electron resonances that dominate the low-energy region of the absorption spectrum have provided serious challenges to theorists. These challenges have been largely met through studies involving many-body perturbation theory (MBPT) [1], the *R*-matrix method combined with multichannel quantum-defect theory [2], configuration interaction for the continuum [3], and the hyperspherical-coordinate approach [4]. Although photoionization with excitation certainly occurs for inner-shell photoionization, as confirmed in the cases of argon [5], krypton [6], and xenon [7], the double-electron resonances are not expected to dominate the inner-shell cross sections as seen for valence photoionization where the $ns^2 \rightarrow ns\epsilon p$ cross section passes through a Cooper minimum.

Inner-shell photoionization highlights a different set of many-body interactions, which include interchannel coupling, core relaxation, polarization, and Auger decay. Aside from the purely theoretical interest generated by the complex electron correlation of such systems, accurate models of stellar interiors and the interstellar medium require reliable photoionization cross-section data [8], especially for such notable ''heavy'' elements as magnesium and calcium.

Recently, Henke *et al.* [9] have published a compilation of experimental and semiempirical x-ray absorption cross sections over a wide range of energies including inner-shell photoionization for Mg, Ca, and Sr. It is important to note that the experimental data [9] are based on transmission experiments on solid samples and may not accurately represent atomic photoabsorption cross sections for photon energies near thresholds. On the theoretical front, Chantler [10] has reported results of Dirac-Hartree-Fock calculations providing an important single-particle approximation reference. Inner-shell calculations in the relativistic random-phase approximation (RRPA) [11] have previously been reported for the *L* shell of Mg by Deshmukh and Manson [12] and Nasreen *et al.* [13] and the *M* shell of Ca by Deshmukh and Johnson [14]. A previous theoretical study [15] investigated relaxation effects in penultimate-shell photoionization of Mg, Ca, and Sr using the relativistic random-phase approximation modified to include relaxation effects (RRPAR) but did not examine photoionization from *K* shells or the *L* shell of Ca and did not include the effects of Auger decay. Studies of inner-shell photoionization of neighboring elements Ne [16] and Ar [17] using the relativistic random-phase approximation modified to include effects of relaxation and Auger decay (RRPARA) showed the necessity of including both effects in calculations of *K*-shell electrons. The effect of relaxation on the $3d$ subshell of Sr has been previously studied [15], whereas here we examine many-body effects on *K*- and *L*-shell photoionization.

In addition to the total photoionization cross sections, the partial cross sections for individual channels and the photoelectron angular-distribution asymmetry parameters β also yield insight into many-body interactions. Relaxation effects have been found to considerably alter the branching ratios of partial cross sections and angular-distribution asymmetry parameters [16,18,19]. In the case of photoionization of an inner ns^2 subshell electron in the vicinity of a more dominant np^6 cross section, it may be that the effects of core relaxation of the *ns* hole are only apparent upon examination of the weaker $ns^2 \rightarrow ns\epsilon p$ partial cross section rather than the total absorption cross section.

The purpose of this paper is to consider the role of various many-body effects in inner-shell photoionization of Mg, Ca, and Sr for energies near the respective thresholds. By comparing a sequence of theoretical calculations including Dirac-Hartree-Fock [10], RRPA, RRPAR, and RRPARA, and experimental or semiempirical results [9] (where possible), we can judge the relative importance of interchannel coupling, core relaxation, and Auger decay. In Sec. II, we review the methods of the RRPAR and RRPARA. The results are reported in Sec. III in a shell-by-shell manner. Section IV is a discussion of some of the implications of this work.

*Present address: Department of Physics, University of Central Florida, Orlando, FL 32816.

†Present address: Department of Biochemistry and Biophysics, University of California San Francisco, San Francisco, CA 94143-0448.

II. METHODS

The RRPA developed by Johnson and co-workers [11] is a fully relativistic implementation of the random-phase approximation with exchange (RPAE) [20]. In the RRPA, the partial photoionization cross section for a particular subshell is given by

$$\sigma_{n\kappa}=\frac{4\pi^2\alpha\omega}{3}(|D_{nj\to j-1}|^2+|D_{nj\to j}|^2+|D_{nj\to j+1}|^2), \tag{1}$$

where n is the principal quantum number, ω is the photon energy, and $\kappa=\mp(j+1/2)$ for $j=\ell\pm\frac{1}{2}$, where j and ℓ are the single-electron total and orbital angular-momentum quantum numbers, respectively. The dipole matrix element $D_{nj\to j'}$ is the reduced RRPA dipole matrix element for the photoionization channel $nj\to j'$.

The angular-distribution asymmetry parameter $\beta_{n\kappa}$ for the subshell $n\kappa$ is defined in terms of the differential photoionization cross section as

$$\frac{d\sigma_{n\kappa}}{d\Omega}=\frac{\sigma_{n\kappa}(\omega)}{4\pi}\left[1-\frac{1}{2}\beta_{n\kappa}(\omega)P_2(\cos\theta)\right], \tag{2}$$

where θ is the angle measured between the directions of the incident photon and the photoelectron. When a subshell is split by spin-orbit splitting into two different levels κ and κ', it is conventional to use the weighted average given by

$$\beta_{n\kappa}=\frac{\sigma_{n\kappa}\beta_{n\kappa}+\sigma_{n\kappa'}\beta_{n\kappa'}}{\sigma_{n\kappa}+\sigma_{n\kappa'}}. \tag{3}$$

The RRPAR method approximates the effects of core relaxation by calculating the continuum photoelectron orbitals in the potential of the relaxed ion. The ionic core with the hole in the level with $j=\ell+\frac{1}{2}$ has a lower ionization threshold energy and also represents the most populated of the two levels. Thus, we generally consider the hole to be in the subshell with largest j for the purpose of obtaining the V^{N-1} potential. Overlap integrals of the form $\mathrm{Det}\langle\phi_i'|\phi_i\rangle$ between orbitals of the unrelaxed ground state ϕ_i and the corresponding orbitals of the final relaxed state ϕ_i' are included in the RRPAR dipole matrix element for each electron i of the ionic core. Inclusion of these overlap integrals is important for calculation of the partial photoionization cross sections since they approximately remove oscillator strength due to double-excitation shake-up and shake-off processes from the single-excitation channel oscillator strength [21]. In the RRPARA we approximately include the effects of Auger decay, by adding to the RRPAR dipole matrix element contributions involving overlap integrals between orbitals of the ground state and the continuum orbitals of the final state. For example, in the case of the K shell of Ca, the specific terms added to the RRPAR dipole matrix elements are

$$-\sum_{n=2}^{3}\sum_{j=1/2}^{3/2}\frac{(D_{1s\to np_j'})\langle np_j|\varepsilon p_j'\rangle}{\langle np_j|np_j'\rangle}. \tag{4}$$

TABLE I. Photoionization thresholds (in a.u.) for the various subshells of atomic magnesium, calcium, and strontium. The third column lists the absolute values of single-particle eigenvalues from a Dirac-Hartree-Fock calculation using the code of Ref. [22]. The fourth the fifth columns list experimental thresholds from Refs. [9] and [23], respectively. The fifth column lists the absolute value of the difference between self-consistent-field calculations of total energy of the neutral atom and the ion (ΔE_{SCF}).

Atom	Subshell	DHF	Expt. [9]	Expt. [23]	ΔE_{SCF}
Mg	$1s_{1/2}$	49.126 68	47.885	48.174	48.203 95
	$2s_{1/2}$	3.780 15	3.26	3.55	3.596 01
	$2p_{1/2}$	2.288 30	1.83	2.126	2.079 73
	$2p_{3/2}$	2.276 73	1.82	2.116	2.069 21
	$3s_{1/2}$	0.253 44		0.2810	0.243 21
Ca	$1s_{1/2}$	150.164 28	148.41		148.925 05
	$2s_{1/2}$	16.967 45	16.11		16.546 75
	$2p_{1/2}$	13.731 64	12.85	13.25	13.263 12
	$2p_{3/2}$	13.592 48	12.72	13.12	13.217 99
	$3s_{1/2}$	2.262 05	1.63		2.160 89
	$3p_{1/2}$	1.349 20	0.933	1.274	1.250 06
	$3p_{3/2}$	1.333 80	0.933	1.261	1.235 53
	$4s_{1/2}$	0.196 31		0.2246	0.188 96
Sr	$1s_{1/2}$	595.637 61	591.828		593.596 92
	$2s_{1/2}$	83.146 32	81.447		82.110 60
	$2p_{1/2}$	75.375 92	73.748		74.241 46
	$2p_{3/2}$	72.842 38	71.278		71.729 74
	$3s_{1/2}$	13.959 74	13.18		13.606 69
	$3p_{1/2}$	11.078 02	10.30	10.59	10.719 73
	$3p_{3/2}$	10.672 97	9.922	10.23	10.323 49
	$3d_{3/2}$	5.628 56	4.998	5.292	5.256 10
	$3d_{5/2}$	5.558 16	4.932	5.229	5.189 45
	$4s_{1/2}$	1.948 91	1.43		1.866 21
	$4p_{1/2}$	1.126 415	0.794	1.072	1.048 58
	$4p_{3/2}$	1.079 93	0.746	1.037	1.004 39
	$5s_{1/2}$	0.181 26		0.209	0.174 56

Photoionization thresholds in the strict RRPA model are the Dirac-Hartree-Fock (DHF) eigenvalues. However, experimental thresholds are frequently utilized. In this work we have used DHF eigenvalues as the threshold for RRPA calculations. The DHF eigenvalues were obtained using the Oxford multiconfiguration Dirac-Fock computer code of Grant *et al.* [22] In the RRPAR and RRPARA, we have used the experimental threshold energies [9] although the absolute value of the difference in total self-consistent-field calculation energies of the neutral atom and the ion (ΔE_{SCF}) accounts for much of the correlation for inner-shell ionization and could be used. Table I summarizes the DHF eigenvalues, experimental threshold energies [9,23], and ΔE_{SCF} energies of Mg, Ca, and Sr for comparison.

The RRPA theory predicts results that are gauge independent provided that one has included all possible dipole-excited channels [11]. The present calculations include all dipole-allowed photoionization channels, namely,

$$1s_{1/2}\to\epsilon p_{3/2},\epsilon p_{1/2},$$

$$2s_{1/2} \rightarrow \epsilon p_{3/2}, \epsilon p_{1/2},$$

$$2p_{1/2} \rightarrow \epsilon d_{3/2}, \epsilon s_{1/2},$$

$$2p_{3/2} \rightarrow \epsilon d_{5/2}, \epsilon d_{3/2}, \epsilon s_{1/2},$$

$$3s_{1/2} \rightarrow \epsilon p_{3/2}, \epsilon p_{1/2},$$

$$1s_{1/2} \rightarrow \epsilon p_{3/2}, \epsilon p_{1/2},$$

$$2s_{1/2} \rightarrow \epsilon p_{3/2}, \epsilon p_{1/2},$$

$$2p_{1/2} \rightarrow \epsilon d_{3/2}, \epsilon s_{1/2},$$

$$2p_{3/2} \rightarrow \epsilon d_{5/2}, \epsilon d_{3/2}, \epsilon s_{1/2},$$

$$3s_{1/2} \rightarrow \epsilon p_{3/2}, \epsilon p_{1/2},$$

$$3p_{1/2} \rightarrow \epsilon d_{3/2}, \epsilon s_{1/2},$$

$$3p_{3/2} \rightarrow \epsilon d_{5/2}, \epsilon d_{3/2}, \epsilon s_{1/2},$$

$$4s_{1/2} \rightarrow \epsilon p_{3/2}, \epsilon p_{1/2},$$

and

$$1s_{1/2} \rightarrow \epsilon p_{3/2}, \epsilon p_{1/2},$$

$$2s_{1/2} \rightarrow \epsilon p_{3/2}, \epsilon p_{1/2},$$

$$2p_{1/2} \rightarrow \epsilon d_{3/2}, \epsilon s_{1/2},$$

$$2p_{3/2} \rightarrow \epsilon d_{5/2}, \epsilon d_{3/2}, \epsilon s_{1/2},$$

$$3s_{1/2} \rightarrow \epsilon p_{3/2}, \epsilon p_{1/2},$$

$$3p_{1/2} \rightarrow \epsilon d_{3/2}, \epsilon s_{1/2},$$

$$3p_{3/2} \rightarrow \epsilon d_{5/2}, \epsilon d_{3/2}, \epsilon s_{1/2},$$

$$3d_{3/2} \rightarrow \epsilon f_{5/2}, \epsilon p_{3/2}, \epsilon p_{1/2},$$

$$3d_{5/2} \rightarrow \epsilon f_{7/2}, \epsilon f_{5/2}, \epsilon p_{3/2},$$

$$4s_{1/2} \rightarrow \epsilon p_{3/2}, \epsilon p_{1/2},$$

$$4p_{1/2} \rightarrow \epsilon d_{3/2}, \epsilon s_{1/2},$$

$$4p_{3/2} \rightarrow \epsilon d_{5/2}, \epsilon d_{3/2}, \epsilon s_{1/2}$$

for Mg, Ca, and Sr, respectively.

The inclusion of relaxation effects in the RRPAR and RRPARA photoelectron potentials and use of threshold energies other than DHF eigenvalues leads to differences in calculations performed in the ''length'' and ''velocity'' gauges. Results of calculations of cross sections presented in this paper will normally appear as the geometric mean of length and velocity results because the geometric mean is less sensitive to ground-state correlations [24].

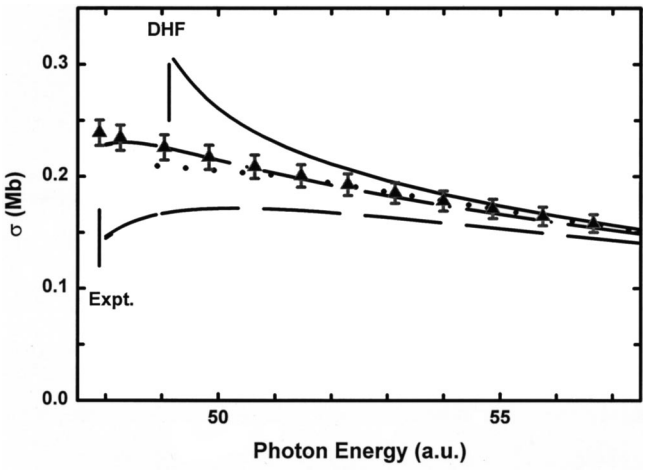

FIG. 1. Total photoionization cross sections of magnesium above the *K*-shell threshold. The dotted line represents Dirac-Hartree-Fock calculations of Ref. [10], the solid line represents the RRPA, the dashed line is the RRPAR, and the dot-dashed line is the RRPARA. The semiempirical data from Ref. [9] are represented as solid triangles. The Dirac-Hartree Fock eigenvalue (DHF) and the experimental threshold [9] are indicated by vertical lines.

Regions just below thresholds where autoionizing resonances may dominate the cross section have not been dealt with in this work. A combination of RRPA dipole matrix elements and the relativistic multichannel quantum-defect theory could be used to study these interesting and complex regions in the absorption spectrum.

III. RESULTS

A. Magnesium

1. 1*s subshell*

The total photoionization cross sections above the *K*-shell threshold of magnesium are shown in Fig. 1. The semiempirical data are from Henke *et al.* [9] and represent the total x-ray absorption cross section. The theoretical models shown in Fig. 1 include the single-particle Dirac-Hartree-Fock calculations of Chantler [10], the RRPA, the RRPAR, and the RRPARA.

Very close to the *K*-shell threshold, where many-body effects are expected to be most notable, the DHF calculations [10] predict a cross section only slightly below the semiempirical values and the RRPA calculations yield a cross section that is clearly larger than the semiempirical values. Including relaxation effects in the RRPAR significantly reduces the RRPA cross section near threshold, even changing the sign of the slope of the cross section. However, the additional inclusion of terms accounting for overlap integrals between orbitals of the neutral ground-state atom with the continuum orbitals of the relaxed ion [see Eq. (4)] in the RRPARA leads to excellent agreement between theory and the semiempirical result. Similar many-body effects were noted previously for *K*-shell photoionization of Ne [16] and Ar [17].

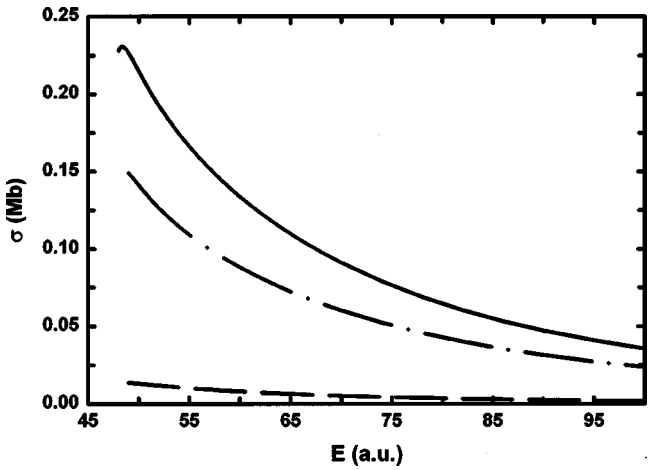

FIG. 2. RRPARA photoionization cross sections of magnesium above the *K*-shell threshold. The solid line represents the total photoionization cross section. The dot-dashed line represents the partial 1*s* cross section. The dashed line represents the sum of all other single-excitation-channel cross sections in the vicinity.

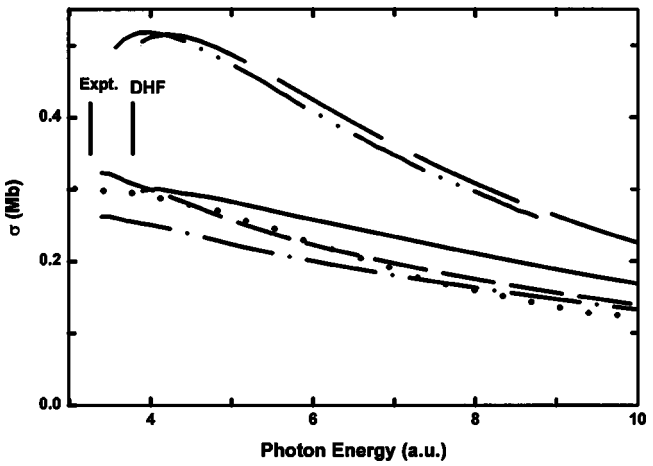

FIG. 3. Partial 2*s* photoionization cross sections of magnesium. The dotted line represents Hartree-Slater calculations [12]; the dash-double-dotted line represents Hartree-Fock calculations [1]; the long-dashed line represents Dirac-Hartree-Fock calculations, the solid line represents RRPA, the short-dashed line represents RRPAR; and the dot-dashed line represents RRPARA. The Dirac-Hartree-Fock eigenvalue (DHF) and the experimental threshold [9] are indicated by vertical lines.

At energies well above threshold, the frozen-core models (i.e., Dirac-Hartree-Fock and RRPA models) should provide reliable cross sections since the photoelectrons have greater kinetic energy and leave the vicinity of the core of spectator electrons before substantial rearrangement can take place. In the limit of high frequency, it is expected that all of the models will converge to the familiar single-particle form (see, e.g., Ref. [25])

$$\sigma(\omega) \propto \omega^{-7/2}; \tag{5}$$

however, it is possible for interchannel-correlation effects to persist even asymptotically [26].

Additional information concerning electron correlation can be obtained by partitioning the total photoionization cross section into various partial cross sections. When a frozen-core potential is used, the sum of partial single-photoionization-channel cross sections effectively account for all double excitation (shake-up) and double photoionization (shake-off) that accompany the ejection of the photoelectron [21,27]. This explains the good agreement between the RRPA and the total absorption cross section [9] well above threshold. An experimental partitioning of the total photoionization cross section, however, would find that the main-line 1*s* partial cross section is lower than that predicted by the frozen-core model because of the transfer of oscillator strength to doubly excited states. Calculations that include core relaxation can approximately account for this flux transfer by the inclusion of overlap integral matrix elements between the initial- and final-state one-electron four-spinors in the transition amplitude. The RRPARA total cross section and various single-excitation partial photoionization cross sections are shown in Fig. 2. The inclusion of overlap integrals reduces the partial 1*s* cross section by approximately 28%, which provides an energy-independent estimation of the amount of absorption due to doubly excited channels. For the 1*s* cross section, we do not present the angular-distribution asymmetry parameters since they vary little from the constant value of 2 predicted by the single-particle model.

2. 2*s subshell*

In the vicinity of the threshold for photoionization of 2*s* electrons, the total absorption is dominated by 2*p*-subshell photoionization which is approximately an order of magnitude larger than the 2*s* partial cross section. Therefore even major modifications of the 2*s* partial cross section due to many-body effects lead to only subtle changes in the total absorption cross section. For this reason, we focus on the 2*s* partial cross sections rather than the total absorption. Calculations of the 2*s* cross section of Mg have been previously reported in single-particle nonrelativistic Hartree-Fock (HF) [1], Hartree-Slater (HS) [12], MBPT [1], and RRPA [12] calculations where it was found that interchannel coupling between the 2*s* and 2*p* channels was very important. Figure 3 shows the 2*s* partial cross sections as calculated in the HS [12], HF [1], DHF, RRPA, RRPAR, and RRPARA methods to underscore the various many-body effects. A comparison of the HS [12] and HF [1] results shows the effect of using the nonlocal-iterative exchange potential in the HF method. The HF and DHF results are nearly identical, showing that relativistic effects are minimal. Comparing the DHF calculation with the RRPA indicates that the effect of interchannel coupling between the 2*p* and 2*s* channels removes oscillator strength from the 2*s* channels. The inclusion of relaxation effects in the RRPAR increases the cross section near threshold. The reduction of the RRPAR partial 2*s* cross section at higher energies relative to the RRPA is due primarily to the inclusion of overlap integrals between orbitals of the ground state and those of the relaxed ionic core, which reduce the cross section by 18.1%. The RRPARA result is similar in its

TABLE II. Absolute values of dipole matrix elements $|D_s|$ and $|D_d|$ and relative phase Δ for $2p$ photoionization in magnesium at 80 eV photon energy. Also, partial cross section for the $2p$ subshell, the $3s$ subshell, and the sum of $2p$ discrete and continuous satellites.

	HS [29]	HF [30]	MBPT [1]	RRPA	RRPAR	Expt. [28]
$\|D_s\|$ (a.u.)	0.214	0.218	0.247	0.2603	0.1978	0.194(17)
$\|D_d\|$ (a.u.)	0.907	0.846	0.854	0.8603	0.7407	0.726(35)
Δ (rad)	4.92	4.82	5.02	5.166	4.823	4.99(16)
σ_{2p} (Mb)			6.25	6.387	4.648	4.46 ± 0.4
σ_{3s} (Mb)			0.093	0.0948	0.0887	0.080 ± 0.011
$\sigma_{2p\ \mathrm{sat}}$ (Mb)					1.078	1.45 ± 0.16

distribution of oscillator strength to that of the RRPA, but has a lower cross section overall due to the same overlap integral reduction as in the RRPAR.

3. 2p subshell

Photoionization of the penultimate subshell of Mg has been previously studied in the Dirac-Hartree-Fock [10], MBPT [1], RRPA [12], and RRPAR [15] methods. The RRPARA cross section is nearly indistinguishable from the RRPAR since there are no *nd* orbitals in the ionic core to participate in the overlap integrals with ϵd orbitals of the continuum. Thus, we do not present a RRPARA calculation of the $2p$ cross section. It is of interest, however, to compare the RRPAR results with the measurements of a so-called ''perfect'' or ''complete'' experiment [28], which determined the absolute values of the dipole matrix elements $|D_s|$ and $|D_d|$ for ϵs and ϵd channels, respectively, and the relative phase Δ at 80 eV. The absolute values of the matrix elements, phase differences, and main-line and satellite partial cross sections in the RRPA and RRPAR are presented in Table II along with the measured values [28] and results of other theoretical approaches [1,29,30] at 80 eV. Table II also compares various partial cross sections at 80 eV. Of course, in the RRPAR, the partial cross sections for satellite channels are energy independent, assuming the ''intensity borrowing model'' [31] where the satellite intensity is predicted by the reduction due to overlap integrals.

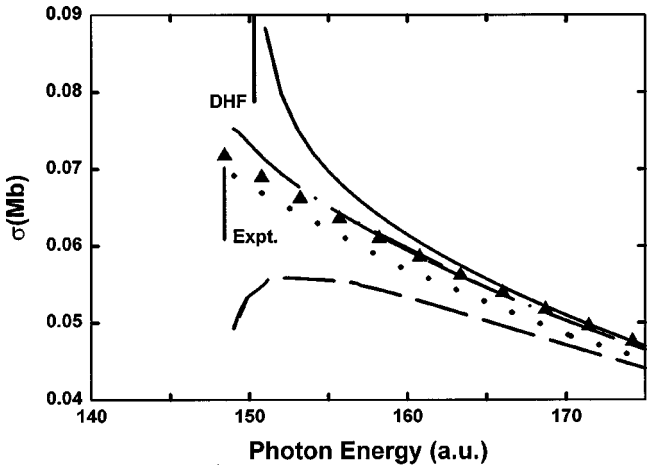

FIG. 4. Total photoionization cross sections of calcium above the *K*-shell threshold. The dotted line represents Dirac-Hartree-Fock calculations of Ref. [10], the solid line represents RRPA, the dashed line is RRPAR, and the dot-dashed line is RRPARA. The semiempirical data from Ref. [9] are represented as solid triangles. DHF and Expt. are the Dirac-Hartree-Fock eigenvalue and experimental [9] thresholds, respectively.

B. Calcium

1. 1s subshell

The total photoionization cross sections above the *K* shell of atomic Ca are shown in Fig. 4. As for Mg, we present the Dirac-Hartree-Fock [10], the RRPA, the RRPAR, and the RRPARA results along with the semiempirical data [9]. Many of the features noted in the discussion of the $1s$ photoionization cross section of Mg are also present in the Ca cross-section calculations. For Ca, the single-particle Dirac-Hartree-Fock cross section [10] is in excellent agreement with the overall shape of the semiempirical cross section [9], although overall the scale is slightly lower. The inclusion of interchannel coupling in the frozen-core RRPA calculations increases the cross section near threshold to levels well above the semiempirical result [9], but yields excellent agreement above 165 a.u. The RRPAR calculations, which include relaxation by constructing separate solutions for the

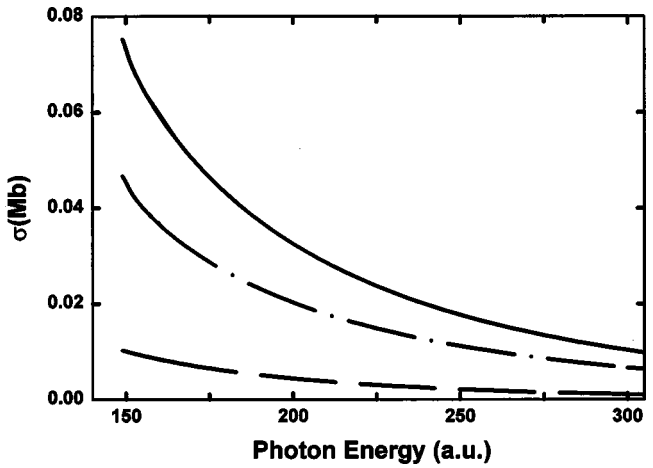

FIG. 5. RRPARA photoionization cross sections of calcium above the *K*-shell threshold. The solid line represents the total photoionization cross section. The dot-dashed line represents the partial $1s$ cross section. The dashed line represents the sum of all other single-excitation-channel cross sections.

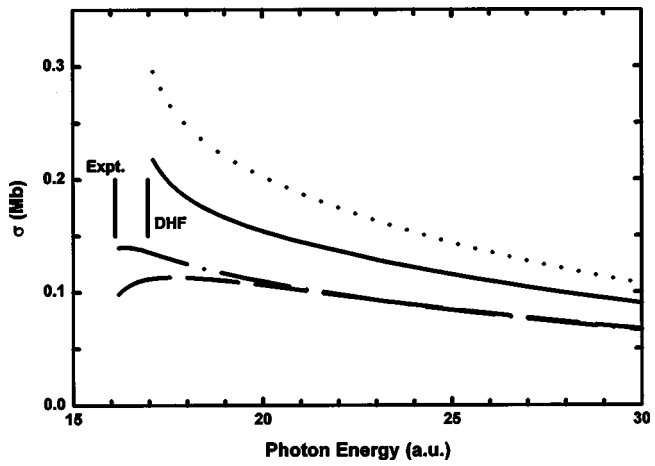

FIG. 6. Partial $2s$ photoionization cross sections of calcium. The dotted line represents Dirac-Hartree-Fock calculations, the solid line represents RRPA, the short-dashed line represents RRPAR, and the dot-dashed line represents RRPARA. The Dirac-Hartree-Fock eigenvalue (DHF) and the experimental threshold [9] are indicated by vertical lines.

ground state and the final $[1s]$ hole state, underestimate the cross section near threshold. The RRPARA calculations, which include relaxation effects and terms involving overlap integrals with continuum orbitals as in Eq. (4), restore the agreement between theory and semiempirical results [9].

Figure 5 shows the total photoionization cross section along with various single-excitation partial cross sections above the *K*-shell threshold of Ca in the RRPARA. In this model, the total cross section is not equal to the sum of the individual single-excitation partial cross sections because of the inclusion of overlap integrals between spectator electrons of the neutral atom and the relaxed ionic core in the partial cross section calculations. The overlap integrals reduce the partial $1s$ cross section by approximately 31%, which is unusually large.

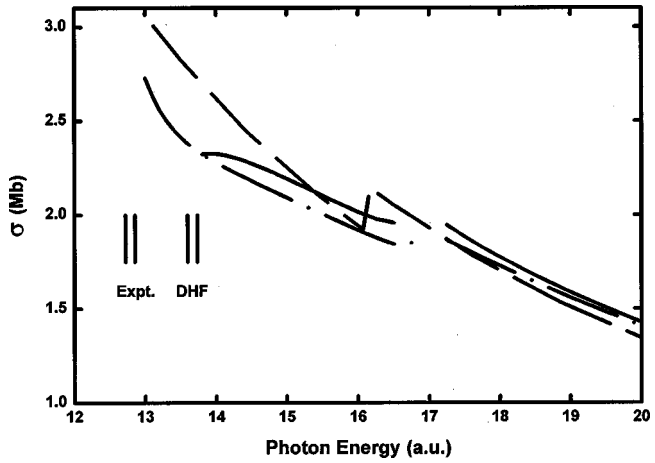

FIG. 7. Total photoionization cross sections of atomic calcium above the $2p$-subshell thresholds. The dashed line is the Dirac-Hartree-Fock cross section of Ref. [10]. The solid line is the RRPA cross section and the dot-dashed line is the result of RRPARA. Experimental [9] thresholds (Expt.) and Dirac-Hartree-Fock eigenvalues (DHF) are indicated by vertical lines.

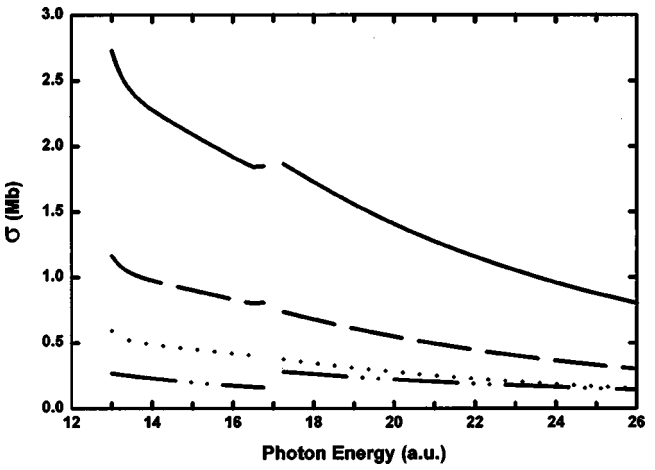

FIG. 8. RRPARA photoionization cross sections of atomic calcium above the $2p$-subshell threshold. The solid line represents the total photoionization cross section. The dashed line represents the partial $2p_{3/2}$ cross section. The dotted line represents the partial $2p_{1/2}$ cross section. The dash-double-dotted line represents the sum of all other single-excitation-channel cross sections.

2. $2s$ *subshell*

The partial photoionization cross sections for $2s$ electrons of Ca are shown in Fig. 6 in the Dirac-Hartree-Fock, RRPA, RRPAR, and RRPARA calculations. The reduction in cross section from the Dirac-Hartree-Fock to the RRPA cross section shows that interchannel coupling with the $2p$ channels removes oscillator strength from the $2s$ channels (as previously noted for Mg). Relaxation effects reduce the cross section near threshold to the RRPAR curve with the overlap integrals among orbitals of the ground-state atom and the ionic core reducing the partial cross section by approximately 25.1%. The inclusion of overlap integrals with the continuum (RRPARA) partially cancels the effects of the relaxed potential near threshold.

3. $2p$ *subshell*

Total photoionization cross sections above the $2p$ thresholds of Ca are presented in Fig. 7 in the Dirac-Hartree-Fock

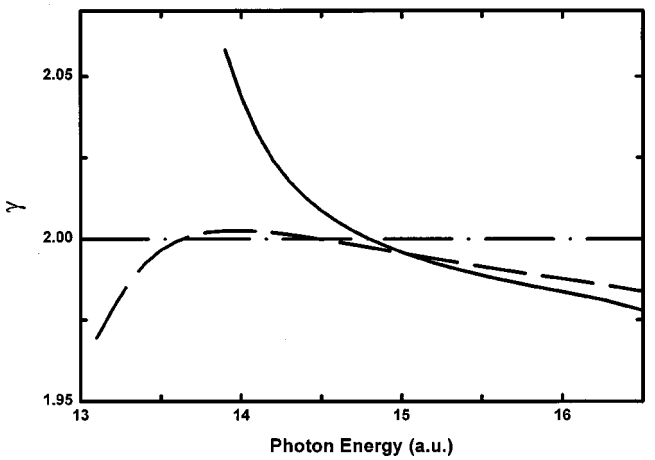

FIG. 9. $2p_{3/2}:2p_{1/2}$ branching ratio γ for calcium in the RRPA (solid line) and RRPARA (dashed line). The statistical ratio of 2.0 is shown as a dot-dashed line for comparison.

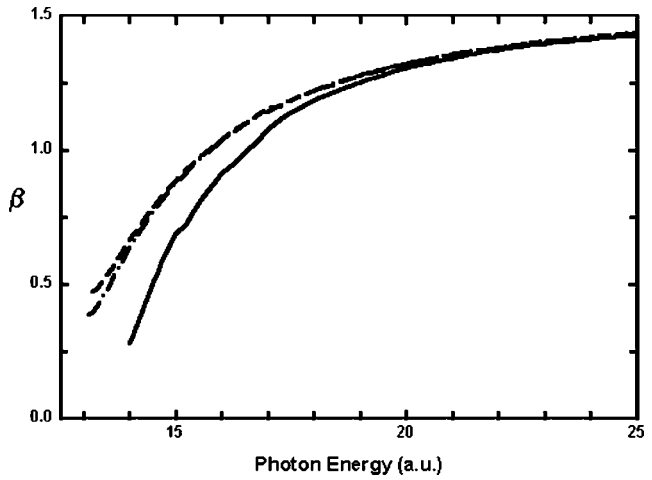

FIG. 10. Photoelectron angular-distribution asymmetry parameter β for $2p$ electrons of calcium. The solid, dashed, and dot-dashed lines represent the RRPA, RRPAR, and RRPARA calculations, respectively.

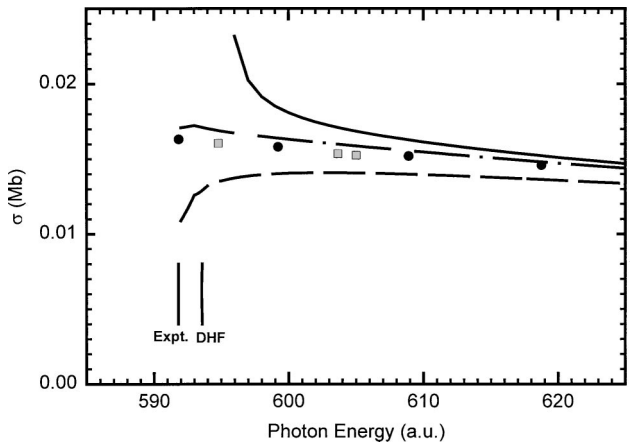

FIG. 12. Total photoionization cross sections of Sr above the *K*-shell threshold. The solid, dashed, and dot-dashed lines represent the RRPA, RRPAR, and RRPARA, respectively. Squares represent Dirac-Hartree-Fock calculations, Ref. [10]. Semiempirical results of Henke *et al.* [9] are shown as solid dots.

[10], RRPA, and RRPARA calculations. The effect of interchannel coupling noted by comparing the Dirac-Hartree-Fock result [10] with that of the RRPA is to reduce the total cross section near threshold. Relaxation effects increase the cross section very close to threshold but slightly reduce it at higher energies. Figure 8 shows the total cross section in the RRPARA and the various main-line partial cross sections. In this model, satellite cross sections are predicted to be approximately 25.9% of the total from the evaluation of overlap integrals between the ground-state orbitals and orbitals of the relaxed ionic core.

Relaxation effects also modify the branching ratio $\gamma = \sigma(2p_{3/2})/\sigma(2p_{1/2})$, as may be seen in Fig. 9. Whereas the RRPA predicts a branching ratio that begins at threshold above the statistical ratio of 2, the RRPAR predicts a branching ratio below 2 at threshold. This can be understood by noting that, in the RRPA (RRPAR), the partial $2p$ cross sections are increasing (decreasing) with increasing energy very near threshold. When the ratio of two cross sections with positive (negative) slope is taken and the $2p_{3/2}$ cross section has a lower threshold than $2p_{1/2}$ due to spin-orbital splitting, the resulting ratio will be larger (smaller) than the statistical ratio. At low energy, the angular-distribution asymmetry parameter for $2p$ electrons, β_{2p}, shown in Fig. 10 is increased by relaxation effects.

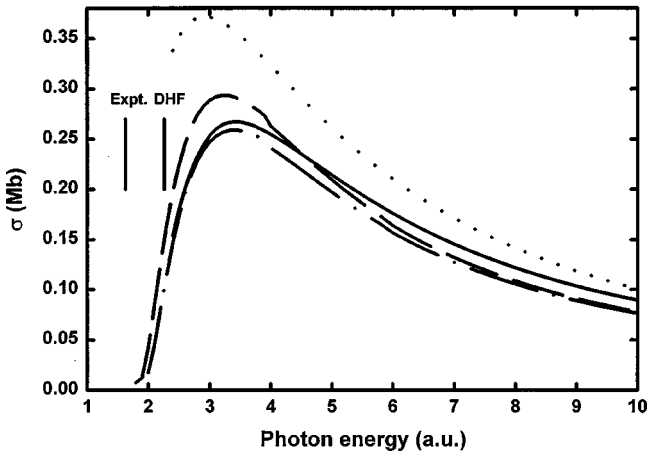

FIG. 11. Partial photoionization cross section of $3s$ electrons in atomic calcium. The Dirac-Hartree-Fock cross section is indicated with a dotted line. The RRPA result is represented by a solid line, the RRPAR with a dashed line, and the RRPARA with a dot-dashed line.

4. 3*s subshell*

The partial photoionization cross sections for $3s$ electrons of Ca are shown in Fig. 11 in the Dirac-Hartree-Fock, RRPA, RRPAR, and RRPARA calculations. The overall shape of the spectrum differs considerably from that seen in Figs. 1 and 4 for the $1s$ cross sections and in Figs. 3 and 6 for the $2s$ cross sections. Interchannel coupling between the $3s$ and $3p$ channels leads to a considerable reduction in the $3s$ cross section in the RRPA as compared to the Dirac-Hartree-Fock calculation. Relaxation effects in the RRPAR increase the cross section near threshold and reduce it at higher energies. The reduction is primarily due to the inclusion of overlap integrals which scale down the cross section by approximately 17%. The inclusion of overlap integrals with the continuum in the RRPARA brings the result back into agreement with the RRPA at low energies.

The photoionization cross section for the $3p$ subshell of Ca was reported in the RRPA and RRPAR elsewhere [15]. Results in the RRPARA are indistinguishable from those in the RRPAR and are therefore not reported here.

C. Strontium

1. 1*s subshell*

With a removal energy of 592 a.u. [9] and an expectation value for orbital radius of only 0.039 a.u., the $1s$ electrons in Sr are tightly bound by the nuclear potential. Yet, *K*-shell

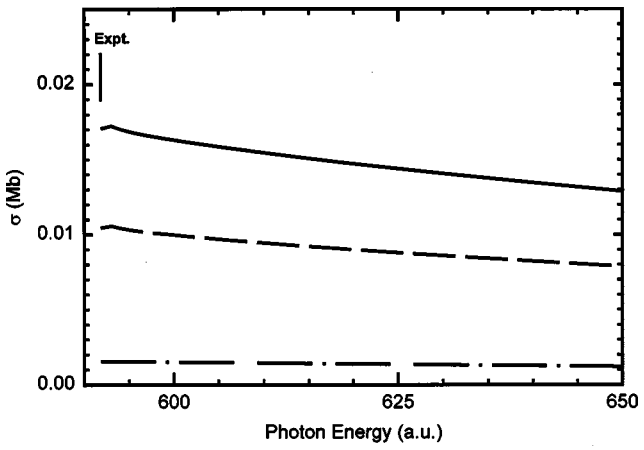

FIG. 13. Total and partial photoionization cross sections for Sr above the *K*-shell threshold in the RRPARA. The solid line represents the total cross section; the dashed line represents the partial 1*s* cross section. All other single-photoionization channels are represented by the dot-dashed line.

photoionization studies of nearby Kr [32] have indicated the need for the inclusion of multielectron effects even for electrons so strongly attracted by the nucleus. Photoionization-with-excitation channels could play an even more important role for Sr with two relatively weakly bound valence electrons than in Kr. This is confirmed by the relatively small overlap integrals between orbitals of the ground state and orbitals of the relaxed final-state ionic core which leads to the prediction that approximately 30% of the total absorption is due to doubly excited channels.

In Fig. 12, we show the results of RRPA, RRPAR, and RRPARA calculations for the total photoionization cross section above the *K* shell of Sr. The RRPA calculation predicts the largest cross section above the DHF threshold, the RRPAR is much lower near threshold, whereas the RRPARA predicts the flattest cross section, in good quantitative agreement with the semiempirical results of Henke *et al.* [9]. The Dirac-Hartree-Fock calculations of Chantler [10] are consistent with the RRPARA results.

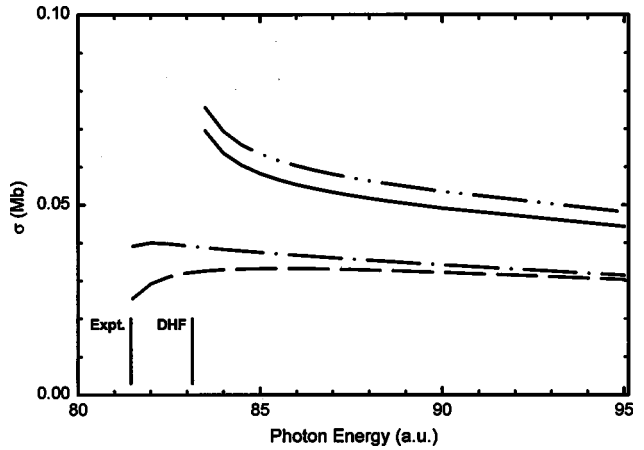

FIG. 14. Partial cross sections for direct photoionization of 2*s* electrons in atomic Sr. The double-dot-dashed line is the Dirac-Hartree-Fock approximation. The solid line is the RRPA result. The dashed line is RRPAR and the dot-dashed line is the RRPARA.

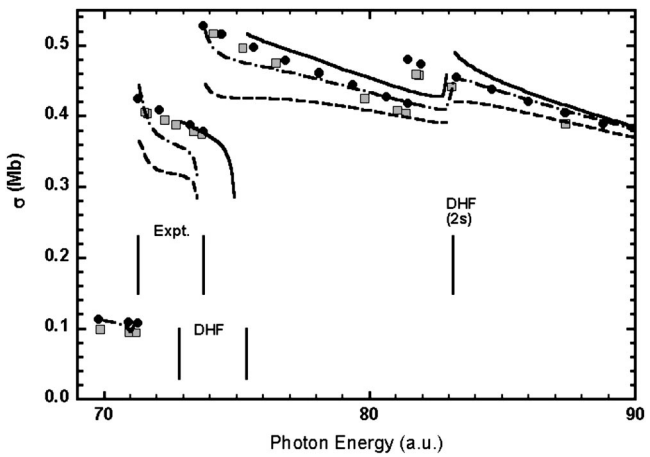

FIG. 15. Sr total photoionization above the 2*p* subshell thresholds. RRPA, solid line; RRPAR, dashed line; RRPARA, dot-dashed line; Dirac-Hartree-Fock of Ref. [10], squares; semiempirical work of Ref. [9], solid dots.

The partitioning of the total cross section into the 1*s* partial cross section and other single-electron cross sections is shown in Fig. 13 in the RRPARA. The large difference between the total cross section and the partial 1*s* cross section is due partly to the cross sections of electrons in shells above the *K* shell, but mostly to the approximately 30% of the oscillator strength arising from doubly excited channels.

2. 2*s subshell*

Above the 2*s* threshold of 81.447 a.u. [9], the photoabsorption cross sections of 2*p* electrons is still approximately an order of magnitude larger than that of 2*s* electrons. To observe the interplay of various many-body effects, we show only the 2*s* partial cross sections in Fig. 14. A comparison of the Dirac-Hartree-Fock calculation and the RRPA result shows that the effects of interchannel coupling between the

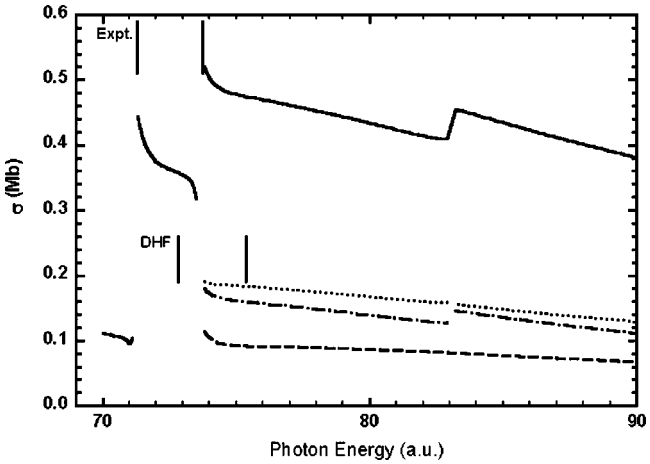

FIG. 16. Partial photoionization cross sections in the vicinity of the 2*p* thresholds of Sr in the RRPARA. The solid line, the total cross section; the dotted line, the $2p_{3/2}$ partial cross section; the dashed line, the $2p_{1/2}$ partial cross section; the dot-dashed line, all other direct single-electron channels.

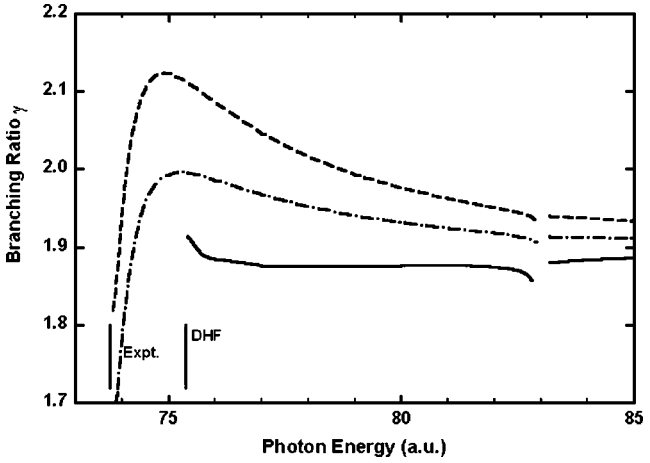

FIG. 17. Branching ratio $\gamma=\sigma_{3/2}/\sigma_{1/2}$ for the $2p$ subshell of Sr in the RRPA (solid line), RRPAR (dashed line), and RRPARA (dot-dashed line). The statistical ratio is shown as a dot-dashed line.

large $2p$ channels and the relatively small $2s$ channels only leads to a small reduction in the $2s$ partial cross section. Relaxation and the inclusion of overlap integrals among core electrons leads to the larger reductions seen the in RRPAR cross section. Fully including overlap integrals with the continuum (RRPARA) leads to a relatively flat partial $2s$ cross section that is approximately 27% lower than the RRPA result at higher energies, leading to the conclusion that shake-up and shake-off are important here as well.

3. $2p$ *subshell*

The threshold energies for photoionization from the $2p_{3/2}$ and $2p_{1/2}$ subshells of Sr are widely split (2.47 a.u.) due to the large spin-orbit interaction (Fig. 15). Core relaxation has a substantial effect on the $2p$ cross section for energies between the two thresholds and just above the $2p_{1/2}$ threshold. Whereas the $2p_{3/2}$ cross section is concave down in the RRPA and RRPARA, it is concave up in the RRPAR. The

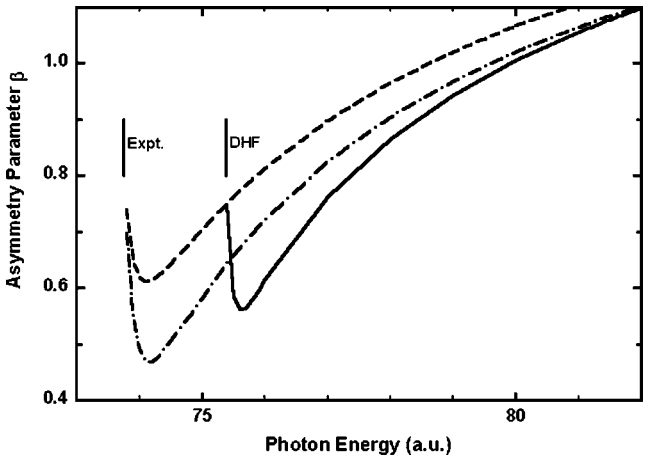

FIG. 18. Photoelectron angular-distribution asymmetry parameter β for $2p$ electrons of strontium. The solid, dashed, and dot-dashed lines represent the RRPA, RRPAR, and RRPARA calculations, respectively.

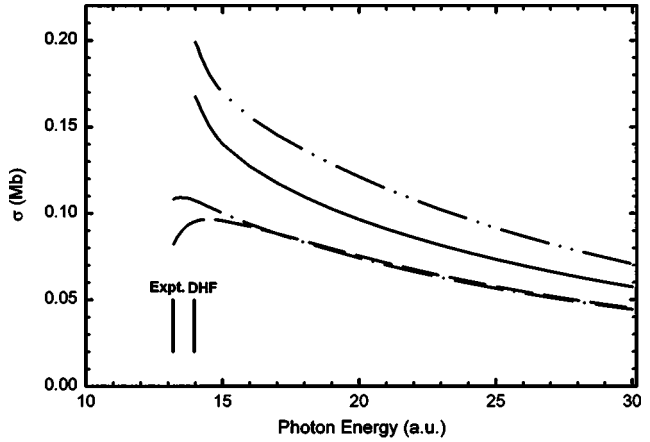

FIG. 19. Partial cross sections for $3s$ photoionization of strontium. The double-dot-dashed line is the Dirac-Hartree-Fock approximation; the solid line is RRPA; the dashed line is the RRPAR; the dot-dashed line is RRPARA.

various subdivisions of the total cross section are shown in Fig. 16 in the RRPAR. The branching ratios $\gamma=\sigma_{3/2}/\sigma_{1/2}$ for the RRPA RRPAR and RRPARA, are shown in Fig. 17. The models differ radically in behavior near threshold with a maximum in γ coinciding with a dip in the $2p_{1/2}$ cross section. The branching ratios remain far from the statistical value of 2 up to photon energies far exceeding the threshold because of the large spin-orbit splitting. The angular-distribution asymmetry parameter for the $2p$ subshell is shown in Fig. 18 where the RRPAR result is found to lie between the RRPA and RRPAR calculations.

4. $3s$ *subshell*

Partial cross sections for the $3s$ subshell of Sr in various approximations are shown in Fig. 19. The effects of interchannel coupling are noted by comparing the Dirac-Hartree-Fock calculation with the RRPA results. The effect of interactions with the $3p$ subshell is to reduce the $3s$ cross section

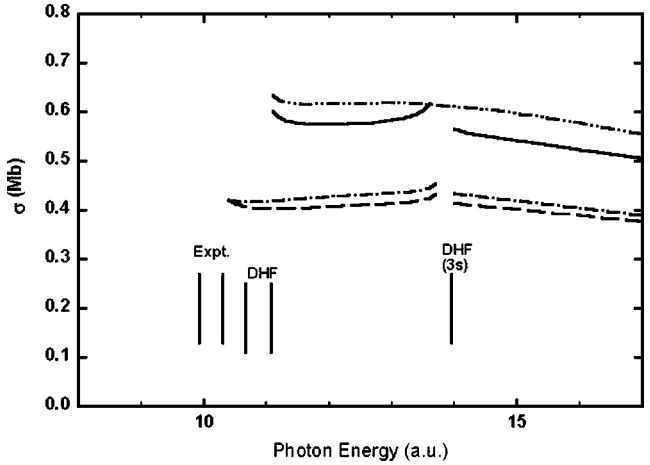

FIG. 20. Partial photoionization cross section of the $3p$ subshell of strontium. The solid line is the RRPA result; the double-dot-dashed line is the Dirac-Hartree-Fock; the dashed line is the RRPAR; the dot-dashed line is the RRPARA.

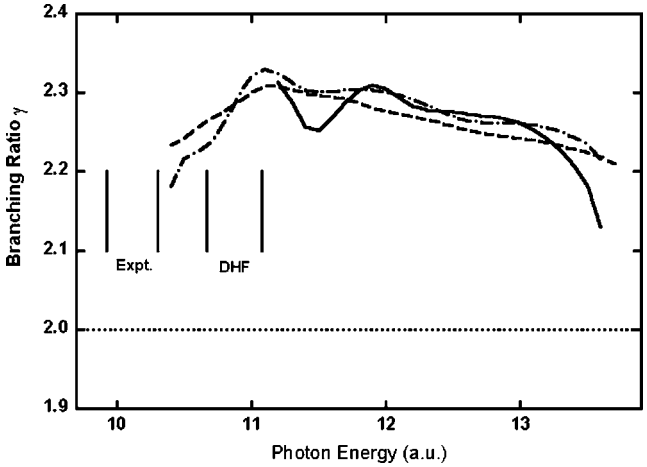

FIG. 21. Branching ratio $\gamma=\sigma_{3/2}/\sigma_{1/2}$ of $3p$ subshell of Sr. The solid line is RRPA result; the dashed line is the RRPARA; the dot-dashed line is the RRPARA. The statistical ratio is 2.

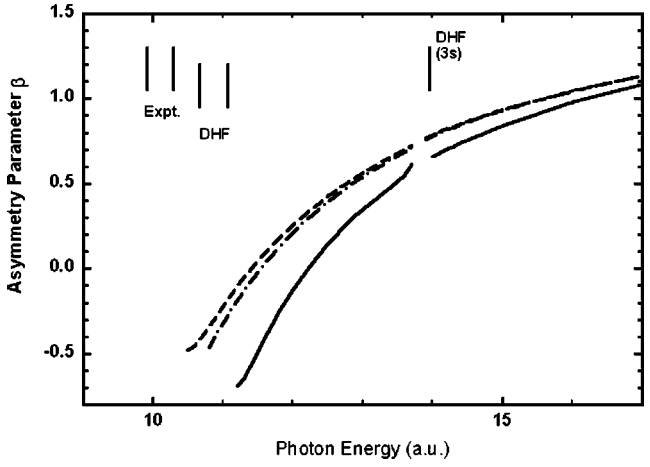

FIG. 22. Photoelectron angular-distribution asymmetry parameter β for the $3p$ subshell of Sr. The solid line is the RRPA; the dashed line is the RRPAR; the dot-dashed line is the RRPARA.

overall. Relaxation effects reduce the $3s$ cross section even further, but near threshold overlap integrals with the continuum orbitals enhances the cross section.

5. $3p$ *subshell*

In the vicinity of the $3p$ threshold, the total absorption is still dominated by photoionization of $3d$ electrons due to the presence of a ''giant resonance'' [15]; thus, to examine the effects of relaxation near the threshold, we consider the partial $3p$ cross section rather than the total cross section. The partial cross sections are shown in Fig. 20. Relaxation effects are seen to be more important than interchannel coupling for the $3p$ subshell; however, many of the differences between the RRPA and RRPAR are due to overlap integrals which reduce the cross section by approximately 23%. The branching ratio for this subshell (see Fig. 21) shows interesting structure and varies substantially depending on the model, but the angular-distribution asymmetry parameter (Fig. 22) is relatively unaffected by relaxation effects.

IV. CONCLUSION

Various many-body effects including interchannel coupling and relaxation have been evaluated for the inner-shell photoionization of magnesium, calcium, and strontium. For the *K* shells it is found that, near threshold, including only interchannel coupling in the RRPA leads to results that are larger than the semiempirical values of Henke *et al.* [9]. The inclusion of interchannel coupling plus core relaxation effects in the RRPAR leads to *K*-shell cross sections that are below the semiempirical values [9]. It is only when overlap integrals between continuum orbitals $\epsilon p'$ calculated in the relaxed ionic potential and the *np* orbitals of the ground-state atom are included as well in the RRPARA that agreement with the semiempirical values is restored. Interestingly enough, the Dirac-Hartree-Fock approximation calculations [10], considered zeroth order in the correlation perturbation, are in very good agreement with the RRPARA results for the *K*-shell total photoionization cross sections of all three elements. Partial cross sections for direct knockout of $1s$ electrons do differ significantly between Dirac-Hartree-Fock and RRPARA models. This is because the RRPARA approximately accounts for the redistribution of oscillator strength to other single- and multiple-excitation channels. Overlap integrals between the orbitals of the neutral atom ground-state wave function and the ionic core final-state orbitals are quite substantial (reducing the partial cross sections by approximately 20%–30%) in each of these cases. This is largely because of the presence of two relatively loosely bound electrons in the valence shell of the alkaline-earth-metal atoms that undergo substantial rearrangement when an inner-shell electron is removed.

Dirac-Hartree-Fock calculations differ significantly from the more sophisticated RRPA-type calculations for the $2s$-subshell channels where interchannel coupling with the $2p$ channels significantly alters the $2s$ partial cross sections. Experimental measurements of partial cross sections of many of these subshells would be very valuable in determining the importance of many-body effects.

The dipole matrix elements and partial photoionization cross sections for the $2p$ subshell of Mg are greatly improved in the RRPAR largely due to the reductions resulting from the inclusion of overlap integrals. The *np* photoionization cross sections are altered in both shape and magnitude by relaxation effects. The change in shape is most apparent in the branching ratio γ, which is sensitive to the initial slope of the cross section. For the deep *np* subshells of Sr, the branching ratio varies far from the statistical ratio of 2 and maintains this variation into high photon energies because of the large spin-orbit splitting.

ACKNOWLEDGMENTS

We wish to thank Walter Johnson for the use of the RRPA computer code. This work was supported by Grant No. PHY-0099526 of the National Science Foundation and by the Office of Scholarly Research of Andrews University.

[1] Z. Altun, Phys. Rev. A **40**, 4968 (1989); Z. Altun, S. L. Carter, and H. P. Kelly, *ibid.* **27**, 1943 (1983).
[2] C. H. Greene and M. Aymar, Phys. Rev. A **44**, 6271 (1991); method based on C. H. Greene and M. Aymar, *ibid.* **44**, 1773 (1991).
[3] T. N. Chang and X. Tang, Phys. Rev. A **46**, R2209 (1992).
[4] C. H. Greene, Phys. Rev. A **23**, 661 (1981).
[5] H. W. Schnopper, Phys. Rev. **131**, 2558 (1963).
[6] S. J. Schaphorst, A. F. Kodre, J. Ruscheinski, B. Crasemann, T. Åberg, J. Tulkki, M. H. Chen, Y. Azuma, and G. S. Brown, Phys. Rev. A **47**, 1953 (1993).
[7] M. Deutsch and P. Kizler, Phys. Rev. A **45**, 2112 (1992).
[8] M. S. Longair, *High Energy Astrophysics*, 2nd ed. (Cambridge University Press, Cambridge, England, 1992), Vol. 1, pp. 89–91.
[9] B. L. Henke, E. M. Gullikson, and J. C. Davis, At. Data Nucl. Data Tables **54**, 181 (1993).
[10] C. T. Chantler, J. Phys. Chem. Ref. Data **24**, 71 (1995).
[11] W. R. Johnson and C. D. Lin, Phys. Rev. A **20**, 964 (1979); W. R. Johnson, C. D. Lin, K. T. Cheng, and C. M. Lee, Phys. Scr. **21**, 403 (1980).
[12] P. C. Deshmukh and S. T. Manson, Phys. Rev. A **28**, 209 (1983).
[13] G. Nasreen, S. T. Manson, and P. C. Deshmukh, Phys. Rev. A **40**, 6091 (1989).
[14] P. C. Deshmukh and W. R. Johnson, Phys. Rev. A **27**, 326 (1983).
[15] M. Kutzner, D. Winn, and S. Mattingly, Phys. Rev. A **48**, 404 (1993).
[16] M. Kutzner and M. Rose, J. Phys. B **32**, 123 (1999).
[17] M. Kutzner, Q. Shamblin, S. E. Vance, and D. Winn, Phys. Rev. A **55**, 248 (1997).
[18] M. Kutzner, P. Pelly, L. Banks, and R. Robertson, Phys. Rev. A **61**, 022717 (2000).
[19] M. Kutzner, P. Pelly, L. Banks, R. Robertson, and L. Caesar, Phys. Rev. A **61**, 062703 (2000).
[20] M. Ya. Amusia, in *Atomic Photoeffect*, edited by P. G. Burke and H. Kleinpoppen (Plenum, New York, 1990).
[21] T. Åberg, in *Photoionization and Other Probes of Many-Electron Interactions*, edited by F. Wuilleumier (Plenum, New York, 1976).
[22] I. P. Grant, B. J. McKenzie, P. H. Norrington, D. F. Mayers, and N. C. Pyper, Comput. Phys. Commun. **21**, 207 (1980).
[23] H. Siegbahn and L. Karlsson, in *Corpuscles and Radiation in Matter I*, Vol. 31 of *Handbuch der Physik*, edited by W. Mehlhorn (Springer-Verlag, Berlin, 1982), p. 215.
[24] A. E. Hansen, Mol. Phys. **13**, 425 (1967).
[25] W. Heitler, *The Quantum Theory of Radiation* (Clarendon, Oxford, 1954), pp. 204–211.
[26] W. B. Dias, H. S. Chakraborty, P. C. Deshmukh, S. T. Manson, O. Hemmers, P. Glans, D. L. Hansen, H. Wang, S. B. Whitfield, D. W. Lindle, R. Wehlitz, J. C. Levin, I. A. Sellin, and R. C. Perera, Phys. Rev. Lett. **78**, 4553 (1997).
[27] C. S. Fadley, Chem. Phys. Lett. **25**, 225 (1974).
[28] A. Hausmann, B. Kämmerling, H. Kossmann, and V. Schmidt, Phys. Rev. Lett. **61**, 2669 (1988).
[29] J. L. Dehmer and R. P. Saxon, Argonne National Laboratories Report No. 8060 Part I, 1973 (unpublished), p. 102.
[30] M. Völkel, Ph.D. thesis, Universität Freiburg, 1988 [reported by V. Schmidt, *Electron Spectrometry of Atoms Using Synchrotron Radiation* (Cambridge University Press, Cambridge, England, 1997), p. 208].
[31] L. S. Cederbaum, W. Domcke, J. Schirmer, and W. von Niessen, Phys. Scr. **21**, 481 (1980).
[32] S. J. Schaphorst, A. F. Kodre, J. Ruscheinski, B. Crasemann, T. Åberg, J. Tulkki, M. H. Chen, Y. Azuma, and G. Brown, Phys. Rev. A **47**, 1953 (1993).